

Determining the Density Profile of Confined Polymer Brushes with Neutron Reflectivity

W. A. HAMILTON,¹ G. S. SMITH,¹ N. A. ALCANTAR,² J. MAJEWSKI,³ R. G. TOOMEY,⁴ T. L. KUHL⁵

¹Center for Neutron Scattering, Oak Ridge National Laboratory, Oak Ridge, Tennessee 37831

²Department of Chemical Engineering, University of South Florida, Florida 33620

³Manuel Lujan Jr. Neutron Scattering Center, LANSCE-12, MS H805, Los Alamos National Laboratory, Los Alamos, New Mexico, 87545

⁴Center for Ocean Technology, St. Petersburg, Florida 33701

⁵Department of Chemical Engineering and Materials Science, University of California, Davis, California 95616

Received 25 November 2003; revised 10 April 2004; accepted 3 May 2004

DOI: 10.1002/polb.20170

Published online in Wiley InterScience (www.interscience.wiley.com).

ABSTRACT: Polymer molecules at solid or fluid interfaces have an enormous spectrum of applications in a wide variety of technologies as lubricants, adhesion modifiers, and protective surface coatings. Because polymer brushes have great potential to be used in such applications, there is a need to determine their structure and efficiency in reduced spaces. Using neutron reflectivity, we have directly quantified the density distribution of opposing polymer brushes under confinement in good solvent conditions under confinement. Our measurements show that the density profile in the overlap region between opposing polymer brushes flattens, consistent with predictions from molecular-dynamics simulations. In addition, a significant increase in the density at the anchoring surfaces due to the collapse of the brush layers was observed. This collapse of the brushes in restricted geometries suggests that high-density brushes do not interpenetrate significantly under good solvent conditions. © 2004 Wiley Periodicals, Inc. *J Polym Sci Part B: Polym Phys* 42: 3290–3301, 2004

Keywords: confinement; diblocks; good solvent; neutron reflectivity; thin films; polystyrene

INTRODUCTION

Polymer molecules at solid or fluid interfaces have an enormous spectrum of applications in a wide variety of technologies. For example, they provide a mechanism for imparting colloid stabilization, they are used as protective coatings (including the mechanical protection of solids

against friction and wear), they govern the interactions of biological cell surfaces, and through judicious design they are used to modulate dispersion properties (e.g., rheology) under a variety of processing conditions.¹ Therefore, knowledge of the conformations that adsorbed or terminally anchored chain molecules adopt when subjected to confinement and/or solvent flow is essential for predicting the interaction forces, tribological, and rheological properties in thin-film technologies.²

In this work, we focus on the behavior of diblock copolymer chains in a selective solvent, in

Correspondence to: T. L. Kuhl (E-mail: tilkuhl@ucdavis.edu)

Journal of Polymer Science: Part B: Polymer Physics, Vol. 42, 3290–3301 (2004)
© 2004 Wiley Periodicals, Inc.

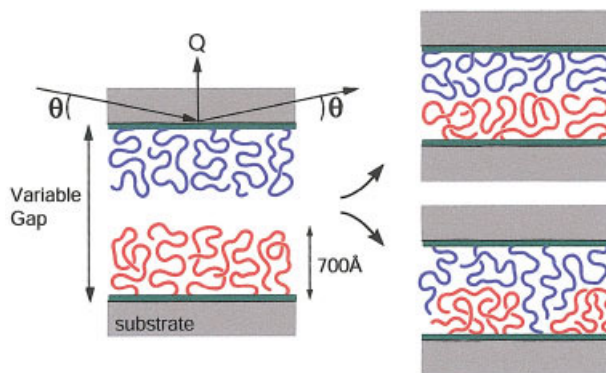


Figure 1. Geometry of the neutron reflectivity measurements and two structural rearrangements of polymer brush layers in contact: brush compression and brush interpenetration. The confinement of two opposing brush layers is likely to be a combination of compression and interpenetration.

which one end of the polymer block anchors the chain to the surface and the other block extends away from the interface into the solution. As shown schematically in Figure 1, when two opposing brushes are brought into contact, two processes may occur simultaneously: interpenetration and compression. Depending on the outcome, the adhesion, lubrication, or shear behavior between the surfaces may be greatly altered. As a result, the ability to predict the structure of polymeric surface coatings under confinement and/or shear is essential for their rational design. Experimentally, information regarding the structure of grafted polymer layers has been deduced from force measurements with equipment such as surface force instruments³⁻⁷ and various scanning probe microscopy techniques.⁸⁻¹² Such force profile and topography measurements have provided important information, but extracting the polymer structure is difficult from such measurements. In many cases, our understanding and interpretation of experimental data have evolved from theoretical studies based on scaling arguments,¹³⁻¹⁷ mean-field theories,¹⁸⁻²⁴ and computer simulations.²⁵⁻²⁸

At the molecular level, neutron reflectivity experiments have been very successful in providing detailed density distribution profiles of polymeric materials at single interfaces (depth profiling); the structure of adsorbed diblock polymers in good, theta, and poor solvents has been investigated as a function of the grafting density.²⁹⁻³⁹ [Neutron reflectometry is a surface-sensitive scattering method that takes ad-

vantage of the wave properties of the neutron probe near the condition of perfect reflection from the sample. The reflection of neutrons from a thin film at a surface provides the ability to characterize the thin-film structure with sub-nanometer-level resolution, enabling the thickness, roughness, uniformity, and density profile of the layers normal to a surface to be determined. The major advantages of neutron scattering techniques (e.g., in comparison with X-ray techniques) are (1) that they are free of radiation damage, (2) that by the application of contrast matching procedures parts of stratified films may be highlighted or screened out, and (3) that neutrons can penetrate thick substrates to probe the structure of buried interfaces. All three of these features are important for the study of confined polymer layers.] Although depth profiling measurements away from an interface have been highly successful, probing the structure that tethered polymer layers adopt under confinement has proven more elusive. The difficulty lies in the need of ultraflat surfaces of a suitably large surface area for neutron scattering measurements. These surfaces must be closely opposed to separations below a few hundred nanometers and must be kept aligned and parallel throughout the duration of the measurement to confine the film of interest uniformly. Early work by Cosgrove and coworkers^{40,41} paved the way for the apparatus that we have developed. In their design, large, optically polished quartz flats were forced to closely approach with a hydraulic ram, and intersurface separations of about 100 nm were attained. However, data interpretation proved difficult because a constant surface separation could not be maintained during the course of an experiment.

Recently, we have designed and built an apparatus so that single-crystal substrates of silicon, quartz, or sapphire with areas of up to tens of square centimeters can be kept parallel at controlled and well-defined separations from millimeters to less than 1000 Å.⁴² Preliminary results for the structure of high-density polystyrene-poly(2-vinylpyridine) (PS-P2VP) diblocks confined between sapphire substrates are reported. These studies demonstrate that this experimental technique provides a new method for measuring the density distribution of grafted polymer brush layers under confined geometries.

EXPERIMENTAL

Polymer Brush Layers

We have focused our initial studies on characterizing the structure of high-density polymer brushes formed by the spin coating of 50:50 PS–P2VP diblocks [molecular weight = 122,000, polydispersity = 1.1, poly(2-vinylpyridine) (P2VP) fraction = 0.51].^{39,43} The P2VP portion of the diblock was hydrogenated [hydrogenated poly(2-vinylpyridine) (hP2VP)], whereas the polystyrene (PS) portion could be either hydrogenated [hydrogenated polystyrene (hPS)] or deuterated to take advantage of contrast labeling. Only results with hPS–P2VP layers are reported here. Following the procedure developed by Levicky,⁴³ we prepared uniform polymer thin films by spin coating at 2000 rpm for 30 s on dry, ultraclean sapphire substrates in a clean room environment. The sapphire substrates were pre-cleaned in acetone and isopropyl alcohol, dried, and then cleaned for 10–20 min in 70:30 sulfuric acid/hydrogen peroxide at 100 °C. Afterwards, the substrates were cooled to less than 50 °C before being rinsed with copious deionized water (18 M Ω cm) and dried with clean nitrogen. The spin-coating solution was 0.6 mg/mL PS–P2VP in toluene. The polymer was dissolved in solution with continuous stirring and was prepared at least 24 h in advance. Just before use, the solution was filtered a minimum of three times through 0.45- μ m poly(tetrafluoroethylene) filters. The spin-coated polymer layers prepared in this manner were about 200 Å thick, as determined by ellipsometry, and only films with zero or few holes were used. After the spin coating, the polymer thin films were annealed *in vacuo* at 180 °C for 24 h. The substrates were then cooled to room temperature before their removal from the vacuum oven.⁴³ The glass-transition temperature for both polymers was just over 100 °C.⁴⁴ P2VP preferred to wet the sapphire (oxide) surface, whereas PS segregated to the air interface. After the annealing, an equilibrium alignment of lamellae parallel to the substrate was expected, as shown schematically in Figure 2(A), because of preferential surface wetting and the incompatibility of the PS and P2VP blocks.

A characteristic reflectivity profile for a single, annealed PS–P2VP layer on sapphire in the dry state is shown in Figure 2(B). Simple boxes of constant thickness and scattering length density (SLD) were used to model the PS and P2VP portions of the thin-film polymer bilayer. The interfaces were smeared with an error function.

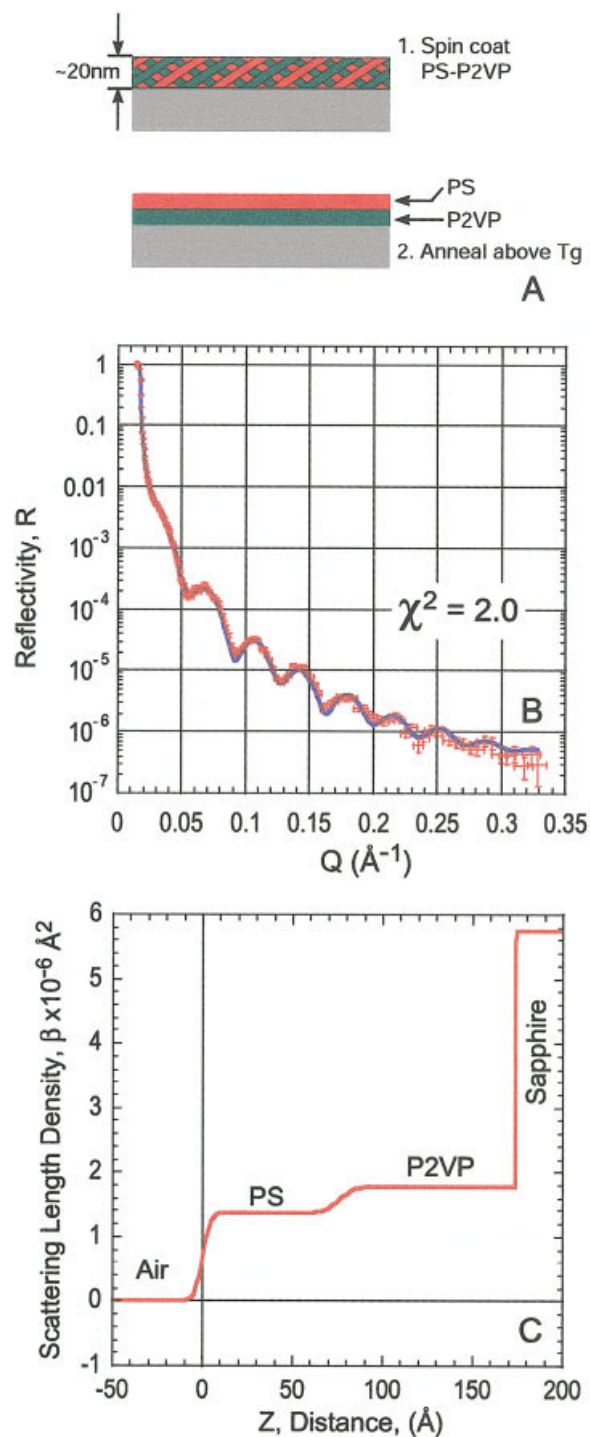


Figure 2. (A) Schematic representation of the spin-coated and annealed PS–P2VP layer and (B) reflectivity profile of a single PS–P2VP layer on a sapphire substrate. The solid curve is a fit to the data based on (C) the SLD profile.

Table 1 lists the calculated bulk SLDs for each material used in these studies. Box model fitting parameters corresponding to the SLD profile in

Table 1. Physical Parameters and SLDs of the Bulk Materials

Material	Chemical Formula	Density (g/cm ³)	SLD ($\times 10^{-6} \text{ \AA}^{-2}$)
Sapphire	Al ₂ O ₃	4	5.8
P2VP	—CH ₂ CH(C ₅ H ₄ N)—	1.11	1.89
PS	—CH ₂ CH(C ₆ H ₅)—	1.05	1.41
Toluene- <i>d</i>	C ₆ D ₅ CD ₃	0.94	5.66

Figure 2(C) are given in Table 2. From the SLD profile, a well-segregated PS–P2VP layer with a bilayer structure is evident. In addition, the fitted roughness of the sapphire substrate was 3 Å, which was consistent with interferograms of the substrates after polishing.

Previously, the structure of 50:50 PS–P2VP layers on silicon substrates was characterized by Levicky et al.,³⁹ and this motivated our own investigations of this system. In these earlier studies, the PS portion of the layer was solvated with a preferential solvent, toluene or cyclohexane, whereas the P2VP portion anchored the solvated PS chains to the substrate. In general, the cross-over from a polymer mushroom regime to a brush regime takes place when the area available per tethered chain (σ) is smaller than the area that an unperturbed coil would adopt ($\sigma^* \propto R_g^2$, where R_g is the radius of gyration). As the area available per chain decreases ($\sigma < \sigma^*$), the lateral crowding of the chains increases. The chains can alleviate this crowding by stretching out and diluting themselves in the solvent. The height (h) of the polymer brush is determined by the balance of the osmotic pressure and the entropic cost of stretch-

ing the chains.^{2,16,17} Because high-molecular-weight 50:50 diblocks were spin-coated onto the substrates, very high-density PS brushes were obtainable. Under these strong, lateral overlap conditions ($\sigma \approx 1/20\sigma^*$), the polymer brush extended $h = 700 \text{ \AA}$ and had a volume fraction of $\phi \approx 25\%$ at the surface. In terms of structure, the polymer brush exhibited a parabolic profile with a flattening of the concentration profile with increasing lateral chain overlap. These results were similar to predictions for strongly stretched brushes based on scaling and self-consistent mean-field theory, in which the flattening of the profile (exponent of 3) underlined the importance of higher order interactions and self-avoidance constraints in polymer/solvent systems.³⁹ In the studies conducted here, similar high-density brushes were formed. To investigate the effect of confinement and compression on the structure of these high-density brushes, we prepared symmetric PS–P2VP polymer layers. The layers on each substrate were assumed to be mirror images of each other and were fixed to have the same SLD, thickness, and functional form.

Table 2. Parameters Used To Fit the Reflectivity Profiles in Figures 2–4

Solvent Gap	PS Thickness	hPS SLD ($\times 10^{-6} \text{ \AA}^{-2}$)	P2VP Thickness	hP2VP SLD ($\times 10^{-6} \text{ \AA}^{-2}$)	Gap Spacing ^a	SLD Gap	χ^2
Single surface	75 Å	1.4	100 Å	1.8	NA		2.4
Air	78 Å	(The polymer layers are symmetric; only layer 1 is reported)			1100 Å	0	2.6
Toluene- <i>d</i>	Parabola	Starting SLD	Ending SLD				
Large gap	200	4.2	5.1	70	1075	5.1	2.5
Small gap	150	3.7	4.6	70	850	4.6	2.8

^a The gap spacing between the substrates has an incoherent smear of 70 Å to account for the waviness of the substrates. Although the surfaces are parallel, over an area (cm²) there is a small variation in the long-range flatness of the substrates ($\lambda/25$). As a result, this variation of 70 Å in substrate separation over the entire region of the beam footprint adds incoherently and must be accounted for in the modeling of the reflectivity profile. The gap-spacing waviness is less than that of the isolated substrates because of conformational deformations.

All interfaces have been smeared by 1–4 Å with an error function to account for the roughness of the interfacial layers, with one exception. The interfacial roughness was 15 Å between the P2VP and PS layers.

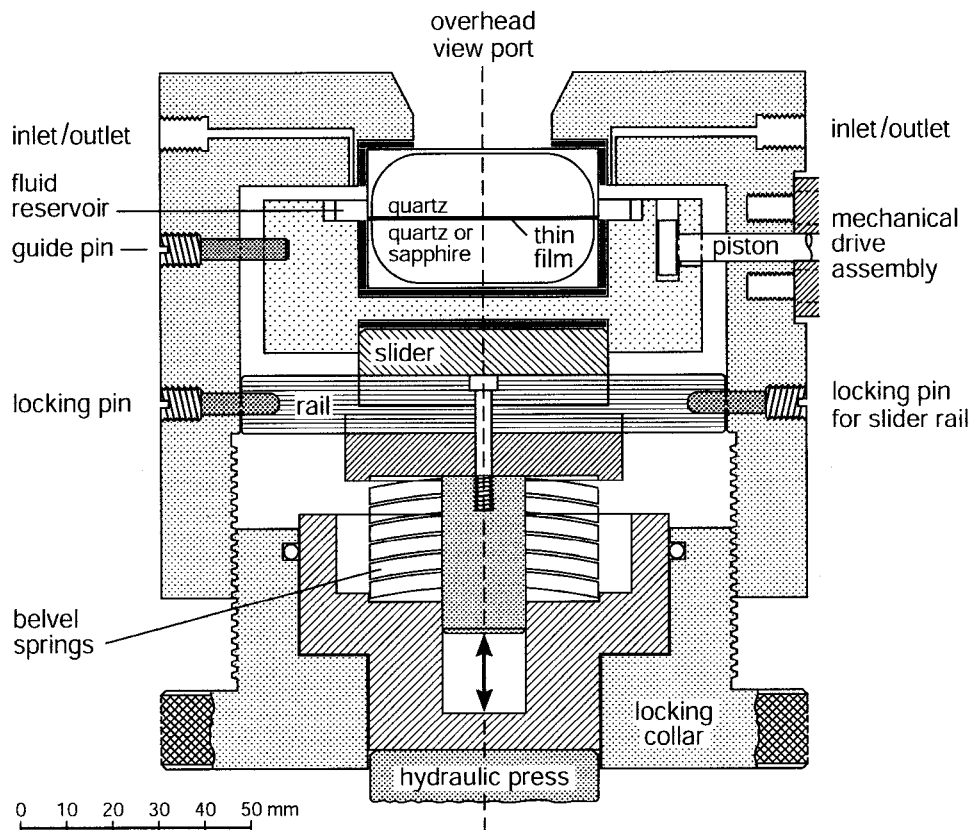


Figure 3. Cross section of the NCC. The neutron beam passed perpendicularly to the view shown. The apparatus was constructed of 304 and 316 stainless steel, and all inlets and outlets were sealed by Teflon o-rings or gaskets. A hydraulic ram could be used to apply high loads, which were calibrated by the measurement of the compression of Belleville washers of variable spring constants. The upper quartz substrate mounted into the top of the outer housing. The lower substrate mounted on a mechanical slider and could be translated (sheared) with respect to the upper surface with a mechanical motor drive assembly.

Neutron Confinement and Shear Cell

A schematic of the apparatus is shown in Figure 3.⁴² The frame and interior components of the neutron confinement cell (NCC) were constructed from 304 and 316 stainless steel. All inlets, outlets, and openings were sealed with Teflon gaskets or o-rings, and this enabled the liquid vapor pressure to be maintained and prevented contamination from entering the chamber. Single-crystal sapphire windows (1 mm thick) acted as beam ports for the incident and reflected neutron beams.

The heart of the device was the substrates used to confine the complex fluid of interest. Theoretically, the minimum gap obtainable with the device was solely a function of the smoothness (waviness) of the substrates used. In other words, the

gap separation was equivalent to the separation between the two substrates. In these experiments, 50-mm-diameter, 15-mm-thick, single-crystal sapphire substrates with a nominal surface waviness of less than $\lambda/25$ over the inner 90% of the surface were used. The outer 10% of each substrate was rounded off to ensure that there would be no edge asperities.

Another critical concern is that these substrates had to be kept in a parallel alignment at a constant gap separation for the duration of the reflectivity measurement (2–12 h). Otherwise, contributions from different substrate separations would tend to smear out the reflectivity profile.^{40,41} In our apparatus, the substrates were mounted into recesses within the steel housing (upper surface) and in the shearing mount (lower

surface). The steel surfaces upon which the substrates rested were machined to a lapped tolerance of less than 10 μin . A Teflon gasket material of Durlon 9000 was placed along the bottom and sides of the substrate recesses to distribute the applied load evenly across the substrate surface. The flexibility of the gasket material and the compliance of the substrate materials enabled the surfaces to conform and self-align. As we show later, very small gap separations were obtained with this construction. The assembled device fit on top of a piston ram, which could be used to apply large normal loads to the substrates through a series of variable-spring-constant Belleville washers. Through the measurement of the deflection of the Belleville washers, the applied load could be accurately determined. A locking collar enabled the applied load to be maintained if the device was removed from the piston ram assembly.

Neutron Reflectivity Measurements

The neutron measurements were made on the SPEAR reflectometer at the Manuel Lujan Jr. Neutron Scattering Center at the Los Alamos National Laboratory. The range of the neutron wavelengths was $\lambda = 1\text{--}16 \text{ \AA}$. The measured perpendicular scattering vector [$Q = (4\pi \sin \theta)/\lambda$] range was 0.008 to about 0.06 \AA^{-1} , where θ is the angle of the incident neutron beam and reflectivities (R) with reasonable statistics could be obtained up to approximately 10^{-6} . Typical counting times were 3–8 h, depending on the beam footprint area. The reflected neutrons were counted with an Ordela 1202N linear-position-sensitive ^3He detector. The data were reduced and plotted as RQ^4 versus Q (this compensated for a sharp Q decrease of the reflectivity due to Fresnel's law). The error bars on the data represent the statistical errors in the measurements (standard deviation); the uncertainty in the Q resolution ($\delta Q/Q$) was nearly constant over this scattering vector range, with a value of approximately 3%.⁴⁵ The neutron reflectivities for various polymer profiles were calculated with the MIRROR program developed by one of us (W. A. Hamilton), which is based on the iterative, dynamical method.⁴⁶ The fits included an additional parameter to normalize the calculated reflectivity to the data.

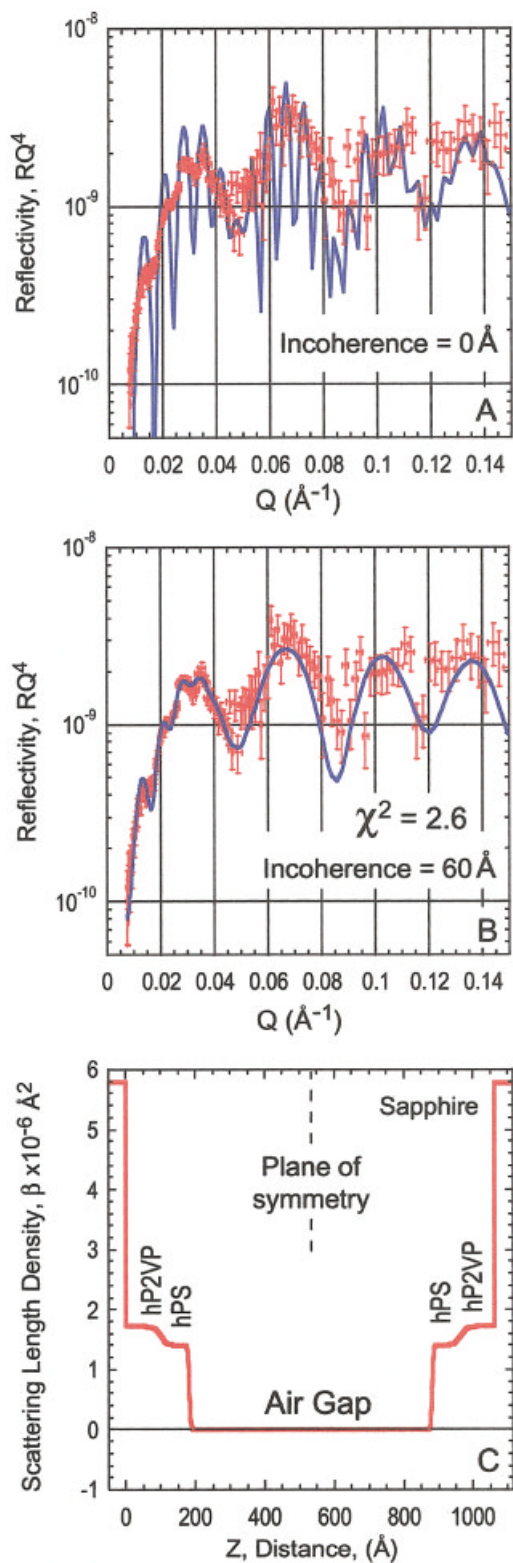
RESULTS AND DISCUSSION

Dry Polymer Films and Incoherent Averaging

In Figure 4, the neutron reflectivity profile and fitted SLD profile obtained from opposing spin-coated polymer layers in the dry, nonsolvated state are shown. The high-frequency Keissig fringes at low Q values clearly indicate that the gap spacing between the substrates is quite small: $D \approx (2\pi)/\text{Fringe spacing} \approx 1200 \text{ \AA}$.³⁰ However, the relatively low visibility of the fringes indicates there is some variation in the separation across the gap. As the beam footprint is about 1.5 cm^2 , this is not unexpected. To account for variations in the intersubstrate separation, we have incoherently averaged the calculated model reflectivity over a Gaussian distribution of gap thicknesses. Parameters for the SLD model are provided in Table 2, and the fitted SLDs match the theoretical values well. The fitted thickness of the PS-P2VP lamellae of approximately 180 \AA matches well ellipsometry measurements conducted just after the spin coating of the layers and the results on a single substrate (Fig. 2). In Figure 4(A,B), the same SLD model has been used to generate the solid curve fits to the reflectivity profile. In Figure 4(A), the gap spacing between the substrates is 1180 \AA . In Figure 4(B), the same gap spacing and SLD model have been used, but the visibility of the fringes has been reduced by the incoherent averaging of the gap spacing with a Gaussian standard deviation of 70 \AA over the sampled area. A root-mean-square variation of 70 \AA in the gap spacing is consistent with the measured flatness of the crystal substrates (peak-to-valley variation $< \lambda/25$, where λ is 6328 \AA); conformal alignment and compression should reduce variations in the gap spacing when the two substrates are closely opposed. Still, macroscopic regions of the sampled area will have small differences in gap spacing, and these will add independently to the total reflected signal. Conversely, treating this variation coherently as a convolution of the SLD profile with a Gaussian smearing function is not appropriate because it would not reduce the visibility of the fringes but rather lead to a reduction in the reflectivity by the Nevot–Croce factor of $\exp[-Q^2\sigma^2]$, where σ is the standard deviation of the smearing function.⁴⁷

The process of incoherent averaging to account for sample variation over macroscopic distances is, of course, similar to incoherent averaging over the uncertainty in the scattering vector, by which

the effect of finite angular and wavelength resolutions on a reflectivity measurement are taken into account. Relaxing the resolution of the in-



strument by about 0.002\AA^{-1} (added in quadrature to the standard instrument resolution), which one might tentatively ascribe to a bending of the opposing crystal surfaces, also blurs out the high-frequency fringes, producing fits of similar apparent quality. However, in the case of resolution averaging, one is correcting for an uncertainty in scale affecting all the dimensional parameters in an SLD profile. Although the flatness of the crystals would lead us to expect an incoherent variation of approximately 100 \AA or approximately 10% in the gap widths here as required by the fits, there is no justification to similarly vary other parameters, such as the surface roughness, polymer layer thickness, and interface width. For example, the fitted SLD profile indicates that the spin-coated layers are quite flat, as expected for such depositions. Likewise, the interfacial roughness between the PS and P2VP portions of the polymer thin film was 14 \AA in the dry state, and the film and substrate roughnesses were 4 \AA or less.

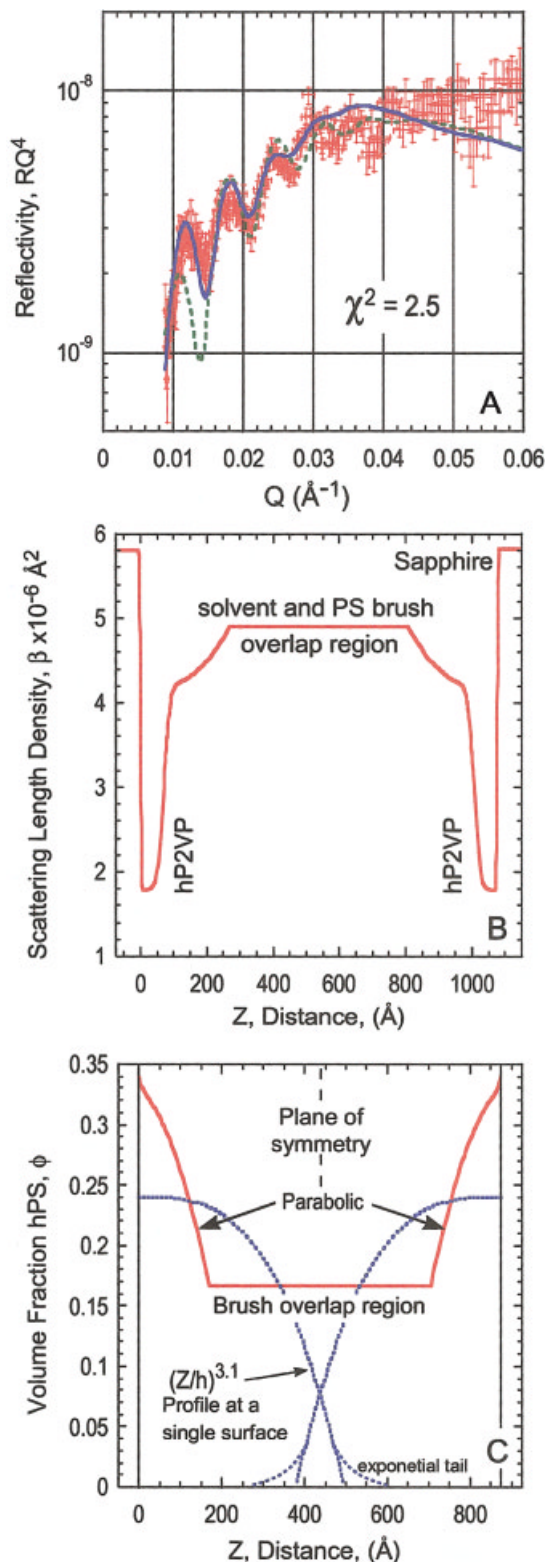
We also note that a uniform contribution to the resolution cannot be caused by an uncertainty in angle due to rippling or bending on a time-of-flight instrument such as SPEAR because at a constant reflection angle it would lead to a constant proportional uncertainty in the scattering vector ($\delta Q/Q \sim \delta\theta/\theta$). Furthermore, the scattering vector uncertainty of 0.002\AA^{-1} on SPEAR at a nominal wavelength of 10 \AA would require bending of the crystal surfaces by approximately 2 mrad ($\sim 0.1^\circ$). This would produce a noticeable broadening of the specularly reflected beam across the position-sensitive detector, but no broadening of this order (which is about an order of magnitude greater than the instrument's angular resolution) has been observed.⁴⁵

In summary, on the basis of the SLD profile in the dry case, well-segregated layers are formed and the bilayer structure is maintained in the NCC with the substrates closely opposed. The

Figure 4. (A) Reflectivity profile for opposing spin-coated PS–P2VP layers. The small Q interference peaks in the profile result from constructive interference between the substrates and their overall separation. The higher Q peaks are due to the polymer layers. The solid curve is a fit to the data based on (C) the SLD profile. The fitting parameters are provided in Table 2. (B) Reflectivity profile generated by the incoherent averaging of the calculated model reflectivity over a 70- \AA Gaussian distribution of gap thicknesses.

total amount of the polymer deposited on each substrate was $\Gamma = 19.7 \text{ mg/m}^2$. A variation of 70 \AA in the gap spacing added incoherently accounts

for the decreased fringe visibility in the measured reflectivity profile. Subsequently, deuterated toluene (toluene-*d*), a good solvent for the PS portion of the diblock, was wicked between the substrates; while maintaining the small intersubstrate separation.



Solvated Polymer Brushes

Under good solvent conditions, the size of a chain scales with $R_g \propto N^{0.6}$, where N is the number of monomers in the chain. The P2VP portions of the diblock chains are anchored to the surface either by direct substrate interactions or through collective interactions with adjacent P2VP chains. Toluene is a nonsolvent for P2VP, and as shown later, there is no evidence of toluene-*d* penetration into the inner 70 \AA of the P2VP film.^{3,39} Assuming there is no net attraction of the PS monomers to the substrate or anchoring P2VP layer, we find that h for the PS brush scales as $h \propto \sigma^{1/3} N$.^{2,16,17} The results from the dry polymer layers in air enabled the amount of polymer to be accurately determined ($\Gamma = 19.7 \text{ mg/m}^2$ and $\sigma = 1/18\sigma^*$). Under good solvent conditions, the PS brush should extend about $h \sim 600 \text{ \AA}$ from the P2VP anchoring layer in the absence of confine-

Figure 5. (A) Reflectivity profile after the wicking of toluene-*d* between the polymer-coated substrates shown in Figure 4. The solid curve is a fit to the data based on (B) the SLD profile. A parabolic profile for the PS portion of the brush at the P2VP interface has been used in the model fitting. The high-density polymer brushes ($\sigma = 1/18\sigma^*$) are compressed and significantly overlap in comparison with the profile of an unconstrained brush at a single interface (the dashed curves have been adapted from Levicky et al.³⁹). The specifics of the physical model used to fit the data are provided in Table 2, and (C) the corresponding volume fraction profile of the PS portion of the brush away from the P2VP anchor layer ($Z = 0$) is shown here. Two important features are evident. First, the polymer brush layers are significantly confined, and this causes the density of the overlap region to increase and flatten, as predicted from mean-field theory and simulations.^{24,25,27} Second, the polymer brush layers are compressed, and this results in a large increase in the brush density close to the P2VP–substrate surface. This increase in the density at the surface implies that the brushes do not interpenetrate to a significant extent. For comparison, the dashed curve in part B is the fit to the reflectivity data based on a flattened brush density profile ($\chi^2 = 4.4$).^{24,25,27}

ment. Representative curves for the density profile of a single, unconfined brush are shown in subsequent figures for comparison.

The reflectivity profile for confined PS brushes in toluene is shown in Figure 5. At low Q values, high-frequency Keissig fringes are still clearly visible in the solvated reflectivity profile and indicate that small gap spacing is maintained under solvation. From the Keissig fringe spacing, the intersubstrate separation is still about $D \approx 1000$ Å. As the two P2VP anchoring portions of the diblock take up almost 200 Å of the total spacing, the remaining $D \approx 800$ Å is available for two opposing PS brushes [$D \approx (4/3)h$]. The brushes are therefore compressed, and their profile is no longer expected to be that of a simple parabolic or flattened parabolic profile as observed at a single surface.

Molecular-dynamics simulations and lattice-model, self-consistent mean-field theories predict that opposing brush profiles will flatten in the overlap region, becoming more uniform as the brushes are compressed, and that significant interdigitation will occur.^{24,25,27} Conversely, if no interdigitation occurs, the brush density profile approaches that derived by the compression of both brushes by an impenetrable wall at their midpoint.²² In modeling these data, we investigated both possibilities. We started with a thin layer to represent the P2VP at each surface, as toluene was not expected to penetrate significantly into the anchor P2VP layer. A parabola was used to represent the PS brush characterized by a thickness, a starting SLD near the hydrogenated P2VP–PS brush interface, and an ending SLD constrained to have the same SLD as the gap region. For moderate compressions, the parabolic profile of each brush was predicted to be largely conserved.²⁵ The gap region was held to a constant SLD, and the gap SLD was allowed to vary from that of pure toluene- d corresponding to the collapse of the brushes to a mixture of PS and toluene- d to account for compression and interpenetration of the brushes. The fitted parameters based on this simple model, which fits the measured reflectivity profile quite well ($\chi^2 = 2.5$), are provided in Table 2 and shown in Figure 5(A) (solid curve). The interfacial region between the P2VP and PS brushes was modeled with an error function (20 Å). As indicated by the constant SLD for the P2VP anchor layer, toluene- d did not penetrate the inner 70 Å of the 100-Å-thick P2VP layer. A mixed toluene- d –P2VP–PS interfacial region therefore extends from this 70-Å layer. For comparison, we also attempted to fit the data with

a flattened profile between the P2VP anchor layers. The flattened profile did not fit the data nearly as well ($\chi^2 = 4.4$) and required the interfacial region between the P2VP and PS portions of the brush to be smeared by 50 Å [dashed curve in Fig. 5(A)].

In Figure 5(C), the volume fraction profile for the solvated polymer brushes based on the model SLD profile is shown; $Z = 0$ corresponds to the portion of the brush extending away from the 70-Å P2VP anchor layer. As the SLDs of PS and P2VP were quite close in value, the volume fraction profile for the brush (ϕ_{PS}) was calculated with the following equation, $\text{SLD}_{\text{fitted}} = \phi_{\text{PS}}(\text{SLD}_{\text{PS}}) + (1 - \phi_{\text{PS}})\text{SLD}_{\text{toluene-}d}$, and the values for the bulk materials in Table 1. An important check of the physical reasonableness of the model fit was verified by the conservation of mass: the amount of the polymer in the solvated case matched to $\pm 2\%$ that found in the dry case, including the solvated portion of the P2VP anchor layer. For comparison, the free, uncompressed, symmetric profile of a PS brush at an interface is shown, based on calculations for the dry polymer layers. There is significant compression of the opposing PS brushes under confinement. At the most simplistic level, the volume fraction profile for overlapping brushes might be expected to be given by the summation of the two uncompressed single-layer profiles. This is not the case. Although the density of the overlapping brush layers is uniform in the center, as predicted from molecular dynamics and mean-field theories,^{24,25,27} there is also a surprisingly significant increase in the concentration of PS at the PS–P2VP interface. This increase in the PS density strongly suggests that the PS brushes compress with confinement and that little interdigitation of the opposing brushes occurs. Indeed, there is surprisingly good agreement between this volume fraction profile and that calculated under the assumption that the two brushes compress and do not interpenetrate.²²

Figure 6 shows the same system at greater confinement and $D \approx 850$ Å intersubstrate separation. For comparison, Figure 6(A) shows the reflectivity profiles, plotted as R versus Q , for both solvated cases. The change in the intersubstrate gap spacing is clearly evident in the low- Q Keissig fringes. A form of the SLD profile identical to that used for the larger separation of 1175 Å was used to fit this reflectivity data. Only the SLD of the parabola used to model the PS brushes and the gap SLD were allowed to vary to accom-

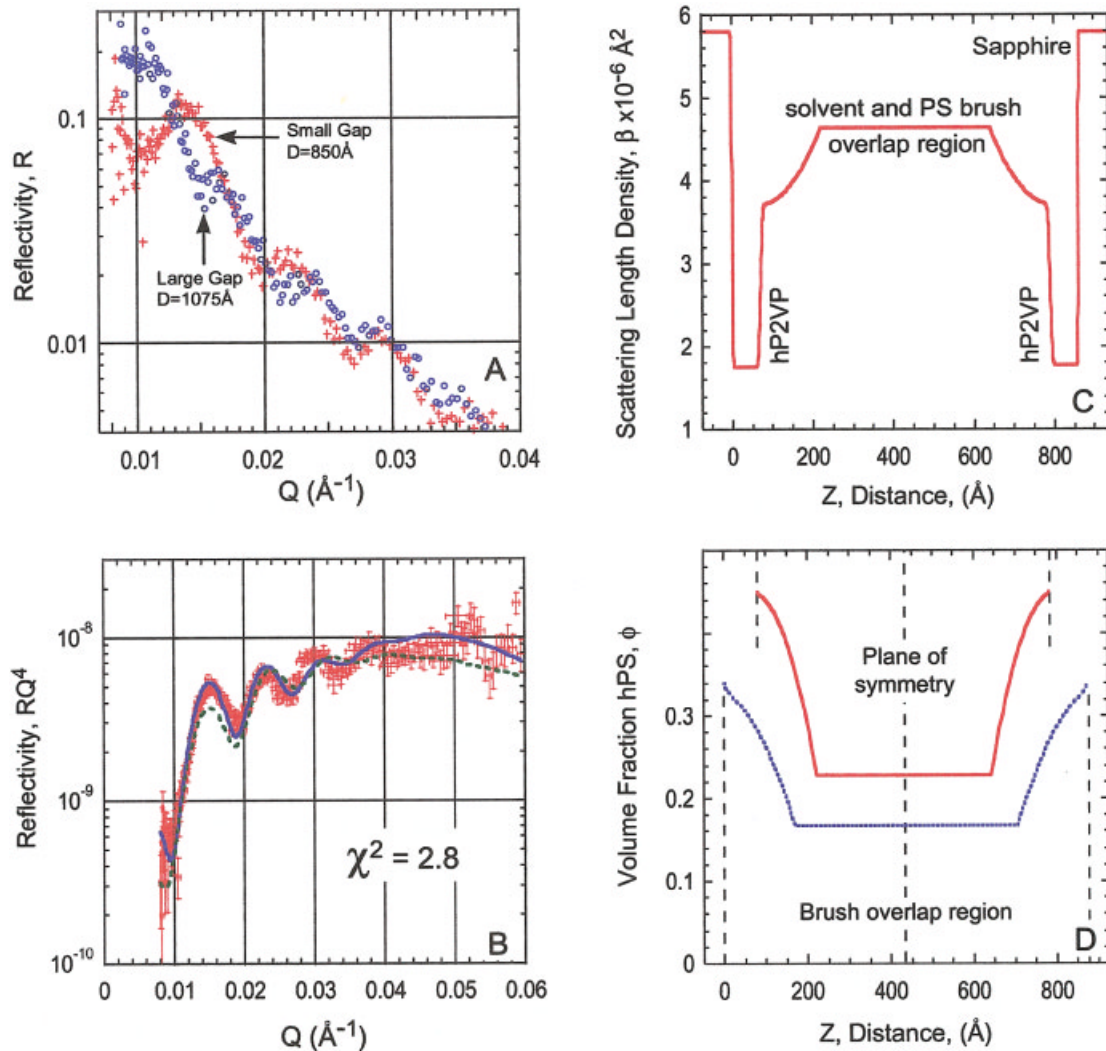


Figure 6. (A) Comparison of the reflectivity profiles for two different intersubstrate separations and (B) the reflectivity profiles at greater confinement ($D \approx 850 \text{ \AA}$). The solid curve is a fit to the data based on (C) the SLD profile. The dashed curve is a fit to the data based on a flattened brush density profile ($\chi^2 = 4.3$). Fitting parameters for the solid curve are provided in Table 2, and (D) the corresponding volume fraction profile of the PS portion of the brush for the intersubstrate separation is shown here and includes the profile from Figure 5. (C) at the larger gap separation for comparison. Again, there is significant confinement of the opposing polymer brush layers, which causes the density of the overlap region to increase and flatten.^{24,25,27} At this greater level of confinement, the density of the PS portion of the diblock further increases at the P2VP–substrate surface.

moderate the squeezing-out of toluene-*d* from between the substrates and changes in the density profile of the more confined PS brushes. The model SLD profile is shown in Figure 6(C). Again, a flattened profile consistent with interdigitation of the opposing brushes did not fit the data nearly as well [Fig. 6(B), dashed curve, $\chi^2 = 4.3$]. A comparison of the volume fraction profiles for the

two different confinement levels are provided in Figure 6(D). Again, a constant amount ($\pm 2\%$) of polymer was obtained, as expected from the conservation of mass. The ability of our simple model to fit both sets of data suggests that the model represents the physical system reasonably well [Fig. 6(B), solid curve]. Additional simulations to better capture the real physical system will pro-

vide insight into the development of more accurate representations of the structure polymer brushes adapt under confinement and are currently being pursued.

CONCLUSIONS

We have used neutron reflectivity to determine the density distribution of opposing polymer brush layers as a function of confinement. The resultant volume fraction profiles are consistent with predictions from molecular-dynamics simulations and mean-field theory, showing a flattening in the overlap region. However, a significant increase in the concentration at the diblock interface is also evident, which has not been previously suggested, and it indicates that the compression of the brushes is more dominant than interdigitation. The power of neutron reflectivity measurements lies not only in the ability to measure the structure of confined polymer films directly but also in the ability to specifically highlight one brush versus the other with contrast variation. In these experiments, the PS portions of the diblock were hydrogenated, whereas the toluene solvent was deuterated. The difference in the SLD of the PS portion in comparison with the toluene solvent enabled the structure of the symmetric PS layers to be measured. In future experiments, asymmetric brushes [in which one substrate has hPS, the other has deuterated PS, and the SLD of the solvent (toluene) is matched to one of the brushes] will enable the profile of a single brush under compression to be measured and the level of compression versus interpenetration to be more fully quantified.

The authors thank Matt Tirrell for graciously providing the poly(2-vinylpyridine)–polystyrene diblocks used in these studies. This work was supported under the auspices of the U.S. Department of Energy through a collaborative University of California/Los Alamos Research grant (9853) and a U.S. Department of Energy Presidential Early Career Award for Scientists and Engineers (PECASE) award (05419-0099-2K). The Manuel Lujan Jr. Neutron Scattering Center is a national user facility funded by the U.S. Department of Energy Office of Basic Energy Sciences–Materials Science under contract number W-7405-ENG-36 with the University of California, and Oak Ridge National Laboratory is managed for the U.S. Department of Energy under contract DE-AC05-00OR22725 with UT-Battelle LLC.

REFERENCES AND NOTES

- Napper, D. H. *Polymeric Stabilization of Colloidal Dispersions*; Academic: London, 1983.
- Milner, S. T. *Science* 1991, 251, 905.
- Hadziioannou, G.; Patel, S.; Granick, S.; Tirrell, M. *J Am Chem Soc* 1986, 108, 2869.
- Taunton, H. J.; Toprakcioglu, C.; Fetters, L. J.; Klein, J. *Macromolecules* 1990, 23, 571.
- Ruths, M.; Johannsmann, D.; Ruhe, J.; Knoll, W. *Macromolecules* 2000, 33, 3860.
- Tsarkova, L.; Zhang, X.; Klein, J.; Hadjichristidis, N. *Macromolecules* 2002, 35, 2817.
- Patel, S. S.; Tirrell, M. *Annu Rev Phys Chem* 1989, 40, 597.
- Overney, R.; Leta, D.; Pictroski, C.; Rafailovich, M.; Liu, Y.; Quinn, J.; Sokolov, J.; Eisenberg, A.; Overney, G. *Phys Rev Lett* 1996, 76, 1272.
- Biggs, S.; Healy, T. W. *J Chem Soc Faraday Trans* 1994, 90, 3415.
- Kelley, T. W.; Schorr, P. A.; Johnson, K. D.; Tirrell, M.; Frisbie, C. D. *Macromolecules* 1998, 31, 4297.
- Yamamoto, S.; Ejaz, M.; Tsujii, Y.; Matsumoto, M.; Fukuda, T. *Macromolecules* 2000, 33, 5602.
- Butt, H. J.; Kappl, M.; Mueller, H.; Raiteri, R.; Meyer, W.; Ruhe, J. *Langmuir* 1999, 15, 2559.
- Alexander, S. *J Phys (Paris)* 1977, 38, 983.
- de Gennes, P. G. *Macromolecules* 1980, 13, 1069.
- de Gennes, P. G. *Adv Colloid Interface Sci* 1987, 27, 189.
- Patel, S.; Tirrell, M.; Hadziioannou, G. *Colloids Surf* 1988, 31, 157.
- Binder, K. *Eur Phys J E* 2002, 9, 293.
- Milner, S. T.; Witten, T. A.; Cates, M. E. *Macromolecules* 1988, 21, 2610.
- Marques, C.; Joanny, J. F.; Leibler, L. *Macromolecules* 1988, 21, 1051.
- Halperin, A.; Zhulina, E. B. *Macromolecules* 1991, 24, 5393.
- Wijmans, C. M.; Scheutjens, J. M. H.; Zhulina, E. B. *Macromolecules* 1992, 25, 2657.
- Wijmans, C. M.; Zhulina, E. B.; Fleer, G. J. *Macromolecules* 1994, 27, 3238.
- Martin, J. I.; Wang, Z. G. *J Phys Chem* 1995, 99, 2833.
- Ruckenstein, E.; Li, B. *J Chem Phys* 1997, 107, 932.
- Murat, M.; Grest, G. S. *Phys Rev Lett* 1989, 63, 1074.
- Murat, M.; Grest, G. S. *Macromolecules* 1993, 26, 3108.
- Grest, G. S. *Adv Polym Sci* 1999, 138, 149.
- Toral, R.; Chakrabarti, A.; Dickman, R. *Phys Rev E* 1994, 50, 343.
- Kent, M. S. *Macromol Rapid Commun* 2000, 21, 243.
- Russell, T. P. *Mater Sci Rep* 1990, 5, 171.
- Penfold, J.; Thomas, R. K. *J Phys: Condens Matter* 1990, 2, 1369.
- Smith, G. S.; Majkrzak, C. F. In *International Tables for Crystallography*, 2nd ed.; Prince, E.; Wilson, A. J. C., Eds.; Kluwer Academic Publishers: Boston; 1999; Vol. C, pp 126–130.

33. Field, J. B.; Toprakcioglu, C.; Ball, R. C.; Stanley, H. B.; Dai, L.; Barford, W.; Penfold, J.; Smith, G.; Hamilton, W. *Macromolecules* 1992, 25, 434.
34. Kent, M. S.; Lee, L. T.; Factor, B. J.; Rondelez, R.; Smith, G. S. *J Chem Phys* 1995, 103, 2320.
35. Perahia, D.; Wiesler, D. G.; Satija, S. K.; Fetters, L. J.; Sinha, S. K.; Milner, S. T. *Phys Rev Lett* 1994, 72, 100.
36. Cosgrove, T.; Luckham, P. F.; Richardson, R. M.; Webster, J. R. P.; Zarbakhsh, A. *Colloids Surf A* 1994, 86, 103.
37. Kent, M. S.; Factor, B. J.; Satija, S.; Gallagher, P.; Smith, G. S. *Macromolecules* 1996, 29, 2843.
38. Karim, A.; Satija, S. K.; Douglas, J. F.; Ankner, J. F.; Fetters, L. J. *Phys Rev Lett* 1994, 221, 33.
39. Levicky, R.; Koneripalli, N.; Tirrell, M.; Satija, S. K. *Macromolecules* 1998, 31, 3731.
40. Cosgrove, T.; Zarbakhsh, A.; Luckham, P. F.; Hair, M. L.; Webster, J. R. P. *Faraday Discuss* 1994, 98, 189.
41. Cosgrove, T.; Luckham, P. F.; Richardson, R. M.; Webster, J. R. P.; Zarbakhsh, A. *Colloids Surf A* 1994, 86, 103.
42. Kuhl, T.; Smith, G.; Israelachvili, J.; Majewski, J.; Hamilton, W. *Rev Sci Instrum* 2001, 72, 1715.
43. Levicky, R. Dissertation, University of Minnesota, 1996.
44. *Polymer Handbook*, 3rd ed.; Brandrup, J.; Immergut, E. H., Eds.; Wiley: New York, 1989.
45. Smith, G. S.; Pynn, R.; Baker, S.; Fitzsimmons, M.; Xuan, L. *Los Alamos Neutron Scattering Center News Lett* 1993, No. 15, p 5.
46. The fitting program used for these data is an eponymous integral data collection and profile modeling analysis package for the MIRROR neutron reflectometer developed by W. A. Hamilton and J. B. Hayter (1992–2003). The statistical and error estimation concepts used therein are described in the following works: (a) Bevington, P. R. *Data Reduction and Error Analysis for the Physical Sciences*; McGraw-Hill: New York, 1969; Chapter 11; (b) Press, W. H.; Teukolsky, S. A.; Vetterling, W. T.; Flannery, B. P. *Numerical Recipes in Pascal*; Cambridge University Press: Cambridge, England, 1989; Chapter 15. The minimization routine employed by the MIRROR program is the downhill simplex method: (c) Nelder, J. A.; Mead, R. *Comput J* 1965, 7, 308. The implementation is described in Chapter 10.4 in ref. 46(b).
47. Nevot, L.; Croce, P. *Rev Phys Appl* 1980, 15, 761.